OPEN ACCESS
IOP Publishing
Measurement Science and Technology
Meas. Sci. Technol. **35** (2024) 125026 (12pp)
https://doi.org/10.1088/1361-6501/ad7a13

Stitching accuracy in large area scanning probe microscopy

Petr Klapetek[1,2,*], David Nečas[2,*], Edward Heaps[3], Bruno Sauvet[4], Vojtěch Klapetek[5], Miroslav Valtr[1,2,*], Virpi Korpelainen[4] and Andrew Yacoot[3,*]

[1] Czech Metrology Institute, Okružní 31, 638 00 Brno, Czech Republic
[2] CEITEC, Brno University of Technology, Purkyňova 123, Brno, 612 00, Czech Republic
[3] National Physical Laboratory, Hampton Road, Teddington, Middlesex TW11 0LW, United Kingdom
[4] National Metrology Institute, VTT MIKES, Tekniikantie 1, Espoo, FI-02150, Finland
[5] Faculty of Science, Masaryk University, Kotlářská 267/2, Brno, 611 37, Czech Republic

E-mail: pklapetek@cmi.cz, mvaltr@cmi.cz, andrew.yacoot@npl.co.uk and yeti@gwyddion.net

Received 29 February 2024, revised 28 August 2024
Accepted for publication 12 September 2024
Published 4 October 2024

Abstract

Image stitching is a technique that can significantly enlarge the scan area of scanning probe microscope (SPM) images. It is also the most commonly used method to cover large areas in high-speed SPM. In this paper, we provide details on stitching algorithms developed specifically to mitigate the effects of SPM error sources, namely the presence of scanner non-flatness. Using both synthetic data and flat samples we analyse the potential uncertainty contributions related to stitching, showing that the drift and line mismatch are the dominant sources of uncertainty. We also present the 'flatten base' algorithm that can significantly improve the stitched data results, at the cost of losing the large area form information about the sample.

Keywords: SPM, stitching, uncertainty, data processing

1. Introduction

The scanning range of commercial scanning probe microscopes (SPM) is typically limited to tens of micrometres and rarely goes above 100 µm. Many industrially relevant samples contain features with sizes that exceed these limited scan ranges. As such, there is an emerging requirement for larger area imaging [1, 2]. For these purposes, specialised commercial metrology systems like the nanopositioning and nanomeasuring machine (NMM) [3] and custom built large area metrological microscopes [4–7] were developed. Another step to bring metrology to this area has been to develop large area high-speed SPM systems with traceable positioning sensors to measure the motion of the positioning stages used in the microscope [8–10].

With control of the scanner's motion together with full knowledge, through measurement, of all scanner movement in all degrees of freedom within the microscope, no specific stitching algorithms are needed and data can be merged in a consistent *xyz* point cloud. However, use of only these instruments, would, in practice, limit large area measurements only to very specialised, complex and expensive but accurate SPMs that measure all movements e.g. with inbuilt interferometers. An alternative is to use a conventional SPM that is equipped with a coarse positioning stage in order to obtain separate images of neighbouring regions. Although these regions may not have a common frame of reference due to imperfect coarse stage positioning, they may be 'stitched' i.e. joined together using algorithms to form one continuous image. If stitching can be used together with an understanding and quantification of the contributions to the measurement uncertainties that are related to the stitching method, large area measurements can be performed with a much wider class of instruments.

Such methods can also easily be used when combined with high-speed SPM imaging, which is designed to provide tens to thousands of full frames per second [11–14]. Individual

* Authors to whom any correspondence should be addressed.

high-speed SPM images are typically small (in the order of micrometers), and more stitching is needed if we want to cover larger areas.

Image stitching is commonly used in various scientific fields, *e.g*, in life sciences [15–18] which include SPM image processing. In most cases, a least squares global optimisation is used to obtain the optimum stitching parameters. Nevertheless, details on the implementation of the stitching process are rarely provided. Moreover, the effects of errors or the handling of scanner imperfections are not quantitatively considered in the literature, and many of the stitching algorithms presented are meant for qualitative imaging and general use without taking into account factors specific to a particular type of instrument.

Usually, the most pronounced systematic imperfection in SPM data is the presence of scanner background, a residual of non-ideal performance of the scanner's linear guidance system, or its imperfect compensation [19–21]. When an individual image is acquired from a scanning probe microscope that uses a tube scanner for lateral motion, this error typically produces a bow in the range of tens of nanometres for lateral scanning in the range of tens of micrometers. It is usually corrected in the data post-processing phase. However, when attempting to stitch multiple overlapping images, the impact of scanner background arises as discussed below in more detail. Moreover, the level of various parasitic errors in high-speed scanners can be larger [22], which makes the potential impact of this effect even more pronounced.

With the current interest in quantitative and correlative microscopy, there is a need to understand and quantify how image stitching may affect the evaluation of results from stitched images and how stitching contributes to measurement uncertainty. In this paper, the details of a stitching implementation in Gwyddion open source software are discussed, including the aspects of determining the scanner background in parallel to stitching as illustrated in figure 1. The accuracy obtained using both simulated and real samples is investigated in order to consider how factors such as image overlap impact the resulting accuracy.

To demonstrate the potential benefits of stitching when used with different classes of metrological instrumentation, three configurations suitable for the acquisition of stitched data were considered:

- Commercial SPM systems with coarse positioning stages and metrological traceability provided via calibration samples,
- A combination of commercial SPMs with upgraded coarse positioning stages featuring traceable sensors and
- Fully interferometric, high-speed large area metrological SPMs.

We also compare the results of stitching on one of the above mentioned experimental configurations with direct large area measurements on a fully interferometric large area metrological SPM system.

2. Experimental arrangement

2.1. Commercial SPM with stepper motor coarse positioning stage

As an example of a commercial instrument, a Dimension Icon SPM from Bruker was used in tapping mode with RTESPA-525 probes. The SPM's stepper motor based coarse motion stage was used to move the sample between locations for individual AFM images. This instrument is located at the Czech Metrology Institute (CMI).

2.2. Commercial SPM with interferometers used to set the position of the coarse positioning stage

National Metrology Institute VTT Mikes (VTT) used a Jupiter XR large sample atomic force microscope (AFM) from Asylum Research. The microscope used stepper motors for the coarse *XY* stage positioning and piezoelectric actuators for *XY* scanning. The AFM has been upgraded to use interferometers to set the position of the coarse positioning stage. Two interferometers for the *XY* axes using two mirrors with a custom designed support for the mirrors have been added to the AFM. The interferometers, type C04 from SmarAct, have a fibre-coupled input and output. The interferometer configuration has been designed to minimise the Abbe error. The custom support ensures that the configuration is still able to accommodate wafers up to 200 mm in diameter. The standard uncertainty of the interferometric measurement was smaller than the pixel size in the acquired AFM images.

2.3. Fully interferometric high-speed metrological SPM

Measurements at the National Physical Laboratory (NPL) were carried out using the NPL high-speed atomic force microscope (HS-AFM) [9]. The HS-AFM comprises a flexure stage that can scan over an area up to $5 \times 5\,\mu m$ at a line scan rate up to 1 kHz in the lateral axes. This high-speed stage is mounted on a three-axis slip stick stage that is used for wide area scanning, coarse positioning and sample approach. The HS-AFM operates in an open loop contact mode using a methodology developed at the University of Bristol [23].

The stage and cantilever position are both measured using NPL designed optical interferometers. The combined lateral position of the high-speed and coarse positioning stages is measured using NPL Plane Mirror Differential Interferometers [24] whilst the cantilever position is measured using a basic Michelson interferometer set up. Because the lateral interferometers are differential, the interferometers measure any relative drift between the coarse and fine stages in the *X* and *Y* axes. The cantilever position measurement is not differential so additional processing is required to remove the high-speed stage background and non-ideal vertical motion in the coarse stage.

For the measurements presented here, the high speed stage was scanned over an area approximately $4.5 \times 4.5\,\mu m$ at either 700 Hz or 1 kHz in the *x* axis and at 1 Hz in the *y* axis. Data was recorded at 2 MHz. Two seconds worth of data was saved

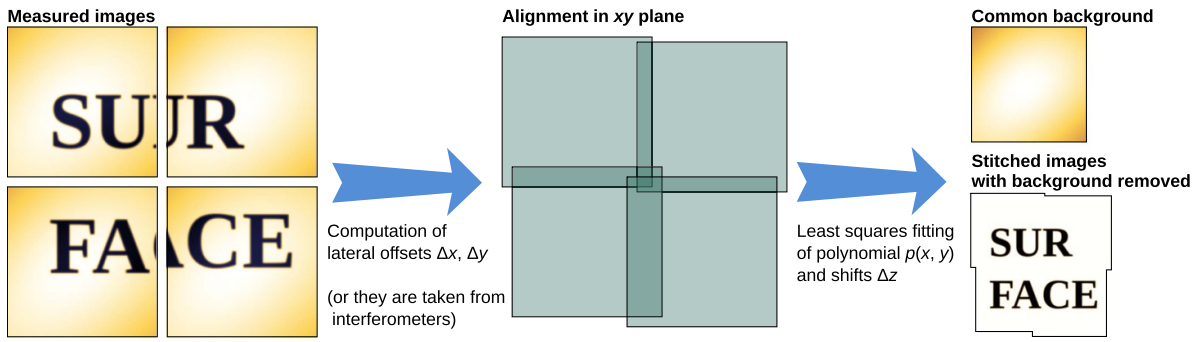

Figure 1. Overview of the stitching procedure.

for each 'frame' meaning there were 4 million data points in each image, giving a lateral resolution of ~3 nm. Data was not recorded whilst the coarse positioning stage was moving.

2.4. Large area SPM

For reference measurements, scanning over large areas without any stitching, a SIOS NMM was used [3]. A total of 4001 profiles were scanned over the area of 550 × 400 µm (resolution was 50 × 100 nm). Measurement was performed in a contact mode using an open hardware controller, Gwyscope [25] and Nanosensors PPP-CONTR AFM probes. Scanning speed was 50 µm s^{-1} hence the overall scan took more than 28 h. The NMM measurements were performed at the Central European Institute of Technology (CEITEC).

2.5. Samples

A 'MetExSPM' sample was measured at CMI and VTT. It was manufactured by Physikalisch-Technische Bundesanstalt in the framework of the EMPIR MetExSPM project as a large area SPM test structure. The sample consists of focused ion beam manufactured structures (logos of MetExSPM project partners) on a silicon substrate.

The samples measured at NPL were a numbered grating and a flatness sample. The numbered grating was produced within the EMPIR BeCOMe project jointly between NPL and the University of Cambridge. It consists of a nominal 25 µm grid with each square on the grid containing a unique pair of hexadecimal numbers to indicate position. The flatness sample was a commercially produced product (NanoSensors FLAT) which is specified to be flat to within 10 nm over a 100 µm area.

3. Methodology

3.1. Data organisation

The data organisation and processing description refer to the implementation in Gwyddion open source software for SPM data analysis [26]; however, the described algorithms are generic and could be applied elsewhere.

SPMs usually store data as a set of points placed on a regular grid and most of the data processing algorithms are designed to work with such data. Even when it is possible to work with general *XYZ* data [27], e.g. on metrological systems featuring interferometers, data is normally rasterised so that the full functionality of Gwyddion can be utilised (some *XYZ* data processing is possible without rasterisation).

In Gwyddion, rasterised SPM data sets that should be processed together are represented as volume data, where each individual layer corresponds to one image in the set (also called an image stack). This creates some limitations: data in the image stack have to have the same physical and pixel resolution, but this limitation simplifies the development of data processing and visualisation routines.

In order to stitch the data, it is necessary to determine the lateral positions of individual frames in the image stack, at least approximately. The image stack has therefore to be accompanied by two datasets (in Gwyddion represented as graph curves) in which the X and Y lateral positions are stored. Such data can be obtained from the coarse positioning stage or from additional interferometers, depending on the instrument.

3.2. Data pre-processing

SPM data can rarely be used without any pre-processing. As a minimum, tilt in the data related to sample mounting and microscope axes orientation has to be removed. When it comes to processing whole image stacks, these methods need to be automated (manual intervention is not possible) and ideally should treat the entire image stack. For these purposes, image stack functions were added to Gwyddion to enable operations such as removal of the mean plane from all the frames or FFT filtering of all the frames in the same way. Such routines can also be used to process data that does not require stitching, *e.g*, when using HS-AFM to investigate the evolution of a sample over time.

A specific automated routine that was used for processing some of the data in this paper is called 'flatten base'. It was found to be very efficient for images of discrete objects on a flat background. The procedure attempts to maximise the sharpness of the dominant peak in the height distribution, which is assumed to correspond to the flat surface. Therefore, a narrower peak means better scanner background removal as a perfectly flat surface would correspond to a δ-function peak.

The sharpness maximisation has two stages, each consisting of several iterations of a levelling operation. The first operation is 'facet levelling' [28], which finds the normal to the surface plane by analysing local normals to the surface and computing their weighted average. For a surface with bars or terraces this is a more suitable strategy than the standard mean plane subtraction. The second operation is polynomial background subtraction with masking. Masking is used to exclude pixels with values greater than three standard deviations larger than the peak mean, assuming they do not belong to the flat base. The background polynomial degree starts at 2 and is gradually increased. The reason for this is that the initial iterations may construct relatively poor masks. However, with a low degree polynomial, the flatness is still improved. Subsequent iterations, with higher degrees, are then also able to better separate the data into a flat base and the object pixels. Importantly, the result of each iteration is accepted only if it makes the dominant peak narrower. Otherwise, the corresponding stage terminates.

3.3. Stitching

If the lateral positions of all the images in the stack were known and all the z values had the same nominal reference plane, data could be stitched easily by placing them on a single large grid. This, however, is usually not the case. Both lateral and z positions can, to some extent, be wrong due to the poor accuracy of the positioning stage, the approach and withdraw cycle between individual images, or drift. The goal of the stitching procedure is to find the ideal placement of the frames to minimise these errors. The procedure is performed separately for the xy and z directions since the xy alignment can be done independently of the z alignment.

The xy alignment has two steps. First mutual xy offsets of all pairs of overlapping images are found using cross-correlation (which is insensitive to the z offsets). The number of overlapping pairs is usually higher than the number of independent offsets. For N images, there are only $N-1$ independent offsets, for instance positions of images $2,3,\ldots,N$ with respect to the first image. The number of overlapping pairs is often close to $4N$, making the problem overdetermined. Therefore, in the second step, independent offsets are found by minimising the ℓ^2 norm of differences between mutual offsets obtained from cross-correlation and mutual offsets computed from the $N-1$ independent offsets, which is a simple least-squares problem.

The z-axis alignment procedure is more complex because it has to simultaneously determine the z offsets and scanner background. It assumes that the xy alignment is already known, as it is normally preceded by xy stitching. Denote $\Delta_{m,n}$ the unknown mutual z-shift between the N images m and n. The shifts $\Delta_{m,n}$ are not independent because $\Delta_{m,k}+\Delta_{k,n}=\Delta_{m,n}$ for all k, m and n. Therefore, we introduce a set of $N-1$ independent shifts Δ_j between consecutive images j and $j+1$, from which $\Delta_{m,n}$ are expressed

$$\Delta_{m,n}=\sum_{j=m}^{n-1}\Delta_j. \tag{1}$$

The common background is described by a polynomial $p(x,y)$ of degree q and it is tied to the position of the scanning system used for the high resolution scan. For an image scanned at location (x_0,y_0) the polynomial representing the common background becomes $p(x-x_0,y-y_0)$.

To find the z-shifts Δ_j and coefficients of the polynomial p, minimise the sum of squares S expressing the mismatch between all pairs of images after z alignment and background subtraction

$$S=\sum_{m,n,x,y}\left[\left(z_{m,x,y}-p\left(x,y\right)-\Delta_{0,m}\right)-\left(z_{n,x+\Delta x_{m,n},y+\Delta y_{m,n}}-p\left(x+\Delta x_{m,n},y+\Delta y_{m,n}\right)-\Delta_{0,n}\right)\right]^2 \tag{2}$$

where x and y $\Delta x_{m,n}$ and $\Delta y_{m,n}$ are lateral offsets between images m and n. In other words, image pixels offset by $\Delta x_{m,n}$ and $\Delta y_{m,n}$ represent the same location on the sample in the two images. The summation is done only over pixels where the images overlap.

Since S is quadratic in the free parameters, z-shifts Δ_j and coefficients of the polynomial p, minimising S is a linear least squares problem. However, the parameters are not independent. The absolute surface height is undefined (arbitrary) and, therefore, one of the z-shifts has to be fixed to obtain a unique solution. Furthermore, the constant and linear terms of p are not independent of the z-shifts and cannot be uniquely determined as any of them can be replaced by a suitable set of z-shifts. It is because the difference $p(x,y)-p(x-x_0,y-y_0)$ is a polynomial of a lower degree than p (by one degree in the general case). Therefore, the constant and linear terms are also excluded from the fitting, reducing the number of free parameters to $(q+1)(q+2)/2-3$. A global mean plane background has to be subtracted after stitching (if required). In total for a polynomial background of degree q we have $N-1+(q+1)(q+2)/2-3$ independent free parameters.

The minimum of S is found by setting the derivatives of S by free parameters to zero. This leads to two types of equations. Differentiating by Δ_i gives for $i\in\{0,1,\ldots,N-2\}$

$$\sum_{m=0}^{i-1}\sum_{n=i}^{N-1}\sum_{x,y}\sum_{j=m}^{n-1}(-\Delta_j)+\sum_{r,s}p_{r,s}P_{r,s}=\sum_{m=0}^{i-1}\sum_{n=i}^{N-1}\sum_{x,y}\left(z_{n,x+\Delta x,y+\Delta y}-z_{n,x,y}\right)\,, \tag{3}$$

where polynomials $P_{r,s}$ are the differences of monomials $x^s y^{r-s}$ evaluated at the two image locations

$$P_{r,s}=\left(x+\Delta x_{m,n}\right)^s\left(y+\Delta y_{m,n}\right)^{r-s}-x^s y^{r-s} \tag{4}$$

for $r\in\{2,3,\ldots,q\}$ and $s\in\{0,1,\ldots,r\}$. For instance, for a 2nd degree polynomial background, $p(x,y)=ax^2+by^2+cxy$ and

$$P_a = 2x\Delta x_{m,n}+\Delta x_{m,n}^2 \tag{5}$$

$$P_b = 2y\Delta y_{m,n}+\Delta y_{m,n}^2 \tag{6}$$

$$P_c \quad = x\Delta x_{m,n} + y\Delta y_{m,n} + \Delta x_{m,n}\Delta y_{m,n}. \tag{7}$$

The x and y summations are always done over the overlap of images m and n (and the sum is empty if images m and n do not overlap). It is necessary to sum for all m smaller than i and all n equal or larger than i to ensure that all unique pairs of images (m, n) that include Δ_i in the equation for their respective heights occur exactly once.

Differentiation by polynomial coefficients $p_{r,s}$ of polynomials $P_{r,s}$ gives the further $(q+1)(q+2)/2-3$ equations

$$\sum_{m=1}^{N-1}\sum_{n=1}^{N-1}\sum_{x,y} P_{r,s}\left[\sum_{j=m}^{n-1}(-\Delta_j) + \sum_{r,s} p_{r,s}P_{r,s}\right] = \sum_{m=1}^{N-1}\sum_{n=1}^{N-1}\sum_{x,y} P_{r,s}\left(z_{n,x+\Delta x,y+\Delta y} - z_{n,x,y}\right). \tag{8}$$

The complete set of equations can be solved for instance using the Choleski algorithm.

4. Results and discussion

4.1. Performance on synthetic data

In order to test the performance of the routines synthetic SPM files representing realistic, but exactly known surface topographies were used [29]. A $50 \times 50\,\mu\text{m}$, 600×600 pixels large surface was generated, featuring different typical objects in SPM data: locally smooth objects generated using the 'partial differential equations', Gwyddion modules (PDEs); random roughness generated using the 'spectral synthesis' module; and a diffraction grating generated using the 'pattern' module. The height scale of the topography was adjusted to set the areal surface texture parameter Sq (root mean square height) to 100 nm roughness of $\text{Sq} = 100$ nm. The generated surfaces can be seen in figure 2. Additionally, a flat surface sample was used.

Image stacks were generated from the synthetic surfaces by cutting them into 4×4 tiles, with defined overlap size. Image stack data were altered by introducing some defects in a defined way, e.g. by adding lateral shift, adding line mismatch, and the whole image stack was stitched back to form a surface area of $50 \times 50\,\mu\text{m}$.

The differences between generated data parameters (topography, roughness, image shifts, polynomial background) and estimated parameters from the stitching process were evaluated. This process was repeated 500 times with random realisations of the introduced defects and the results were statistically analysed.

From the simulations it can be seen in figure 3 that for ideal data, the z stitching errors (including estimation of polynomial background terms) are negligible compared with any SPM uncertainties—even for only 2% image overlaps the relative errors in the polynomial coefficients are below $1 \times 10^{-5}\%$. It should be noted that to obtain the polynomial coefficients in both lateral axes, it is necessary to perform stitching in both lateral axes, otherwise some coefficients are undefined.

When scanning defects are added, as in the case of real images, the stitching errors increase considerably and cannot be ignored. Four types of defects were considered, all affecting the data in the z direction: random noise, line mismatch, random line tilts, and exponentially decaying drift. All these effects can often be seen in SPM data and all but the random noise are removed using a line alignment algorithm. When it comes to data stitching, use of such algorithms would also remove information about the scanner background. Moreover, in many cases, such algorithms must be used with care as they can introduce artificial defects in the data.

To simulate the impact of defects, we used the same synthetic image stack, again divided to 4×4 tiles, but now, after cutting the individual tiles, a particular defect was introduced, individually to each tile. To introduce the line mismatch, we used a random walk algorithm, shifting each fast scan axis profile in z by an amount determined from the previous profile shift and a random number with Gaussian distribution. To introduce the line tilts, each line was tilted independently by some angle, coming from a Gaussian distribution. A z axis drift was added by adding an exponentially decaying value to the height, oriented along the slow scan axis, with the initial value coming from Gaussian distribution and half decay length being a quarter of the image size.

The overall impact of the distortion was evaluated by applying the same process on a flat surface and evaluating the roughness S_q that was introduced by the applied defects. This quantity was used as a measure of the defect impact on the data. By increasing the particular Gaussian distribution widths and evaluating the difference between nominal polynomial parameters and determined polynomial parameters we obtained the relative errors of the determined polynomial coefficients shown in figure 3. We can see that the dominant defects affecting the background estimation are line mismatch and z axis drift. Both these defects mostly affect the y direction parameters of polynomials as they do not disturb the shape of profiles in x direction. The other two defect types, line tilt and uncorrelated noise, have a minor impact on the accuracy, but affect the polynomial coefficients in both directions.

While the polynomial background estimation also works well for very small overlaps, the lateral shift detection is affected significantly more by the overlap size. As the cross-correlation algorithm is used for determination of the lateral shifts of individual image pairs, the overlaps need to have reasonable size compared to the scale of characteristic features. In figure 4 an example of stitching error is shown, demonstrating that the stitching errors are deeply sub-pixel if the image overlap is higher than 15 percent. This depends on sample character—if flat areas with minimum details are in the sample, like on the grating, the stitching errors grow for small overlaps.

4.2. Commercial SPM

To demonstrate the algorithms' performance for processing data from a commercial SPM, 31 images of the MetExSPM sample were measured. The stitched result is shown in

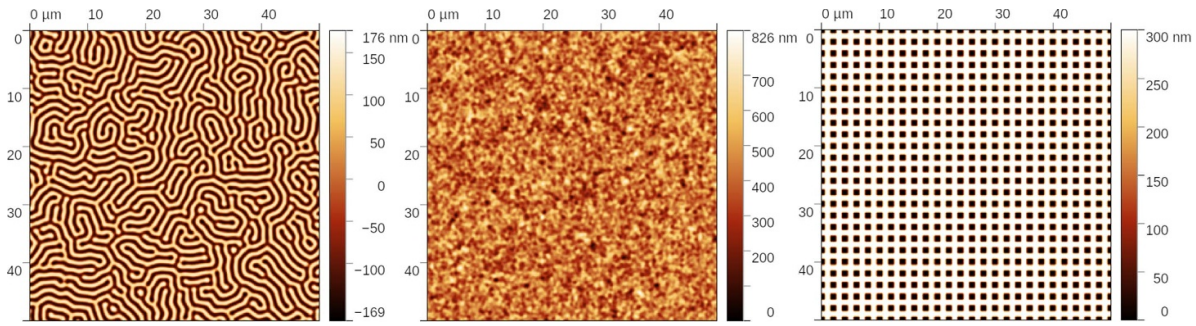

Figure 2. Synthetic data, left to right: PDEs, roughness, grating.

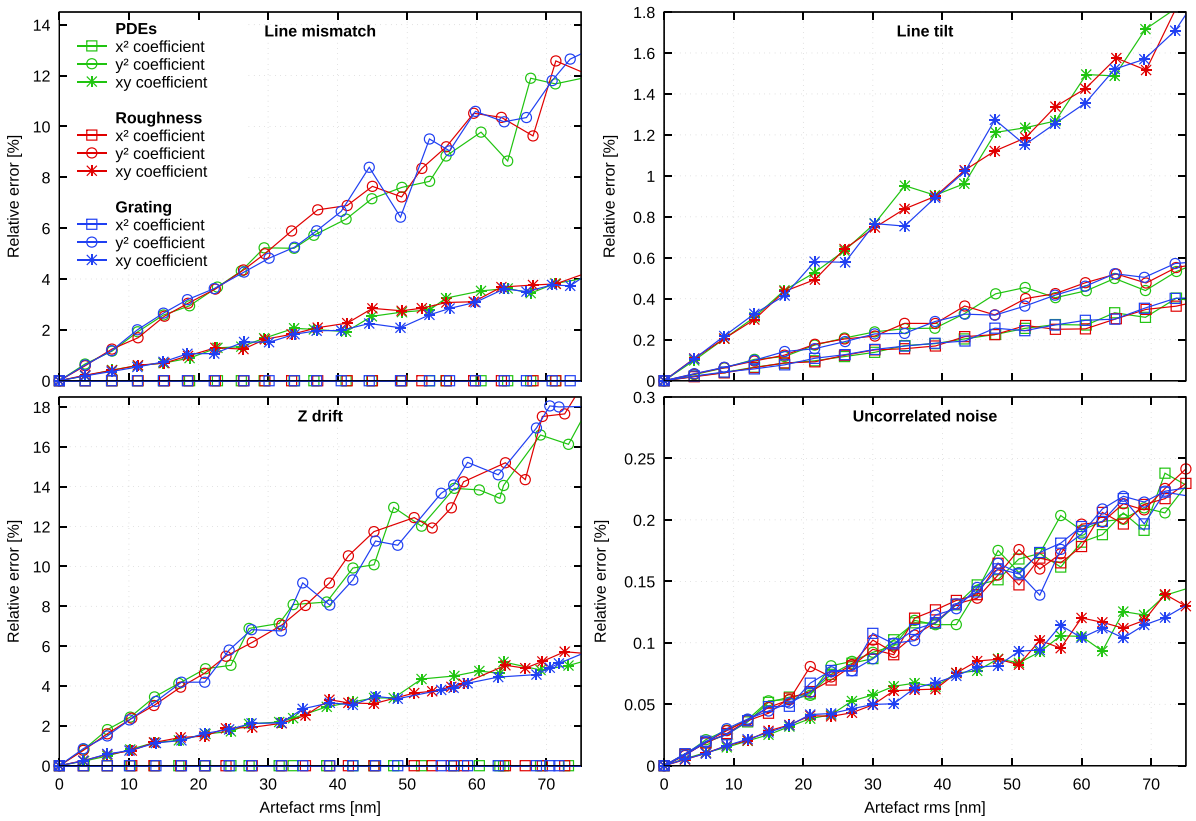

Figure 3. Relative errors of determined polynomial coefficients for 2nd order polynomial background for different defects introduced and different types of surfaces. Image overlap was 1/3 of the frame size, surface roughness is 100 nm.

figure 5(notice that the lateral scale is in millimetres and the height scale is in nanometres).

The lateral image size was $(90 \times 90\,\mu\text{m})$. The frame-to-frame lateral offset was about 70 µm, and was determined by the stepper motors. The lateral positions of the frames determined by stitching showed that the error of the stepper motor positioning was about 300 nm.

To compare the shape of the stitched image with a more accurate measurement, the NMM was used to provide a measurement over the whole sample area without a need to stitch. The residual errors in the z-direction after stitching have a maximum height of 1 nm and are still noticeable as slight discontinuities in the image. These residual errors give an indication of the effectiveness of the stitching routine. After subtracting the two images, residual errors can be seen in more detail; however, the subtracted result was also affected by higher roughness coming from the NMM measurement (1.2 nm S_q on NMM vs. 0.5 nm S_q on the same area when measured by Dimension Icon). Nevertheless, it can be seen that the biggest errors in the stitching process were in the bottom part of the image where the individual images already featured a lot of defects (horizontal lines and jumps).

Using the stitching process discussed above, the scanner background can be analysed as well. In figure 6 the background obtained while stitching the MetExSPM sample data is shown and compared with the background determined directly from repeated measurements on a flat silicon surface and subsequent polynomial fitting of the mean image.

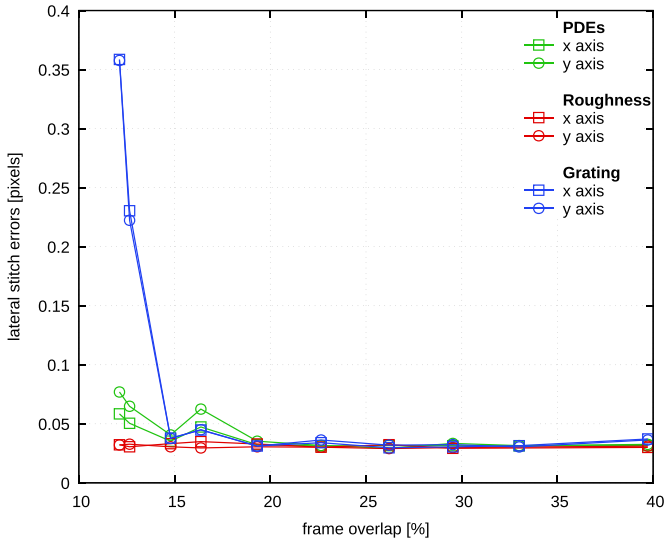

Figure 4. Mean shift errors for lateral stitching for different image overlaps and different types of surfaces.

The parabolic background shape could be expected as a result of some uncompensated residual errors of a tube piezo scanner. It can be seen that the backgrounds are not exactly the same. The biggest problem in data stitching seems to be the presence of z drift which affects the apparent background shape in the slow axis direction. Even if the drift is in the range of nanometres, it affects the determination of the background, which is also in the range of nanometres and could explain the differences observed in figure 6.

On the other hand, when performing the scanner background analysis on a flat surface, slightly different results are obtained (up to 10 nm of difference) even if the analysis is done at different z levels with respect to the full scanner range. As the z drift is typically not the same for all the images in the set, flatten base or other similar algorithm focusing on background removal in each frame independently can be more effective, even if it loses the background information.

Figure 5. Commercial SPM data stitching compared to NMM results. From top to bottom: NMM reference measurement, stitched data from Dimension Icon and difference between them. Red mask shows the areas that were not measured on Dimension Icon.

4.3. Commercial SPM with interferometers

As an example of an upgraded commercial instrument, measurements were performed on a Jupiter AFM equipped with interferometers at VTT (see section 2.2). The same type of sample was used as in the preceding section (MetExSPM structure) and ten images (100 × 100 µm) were acquired with 80 µm separation in x and y.

Figures 7 (A)–(D) show an individual frame, the estimated background and the stitched image using a polynomial background removal and the flatten base algorithm respectively. It should be noted that while the stitching errors are visible in the image, they are less than 2 nm when evaluated from the apparent edges between individual frames.

These stitching imperfections could be attributed to imaging imperfections (drifts, scars, line-to-line jumps) that affected the polynomial background estimation. It can be seen that the estimated scanner background is very different from the background on the commercial microscope discussed in the preceding section, which is related to a different construction of the scanner (separate xy and z axes).

As the slow scan direction was oriented from bottom to top, a large part of the estimated background can be attributed to mechanical or thermal drift after going into contact. By performing stitching without background estimation and using the flatten base algorithm to pre-process the data, stitching residual errors can be reduced to below 0.2 nm, *i.e*, approximately ten times smaller. This, however, means that any real large area background or information about the sample form would be lost.

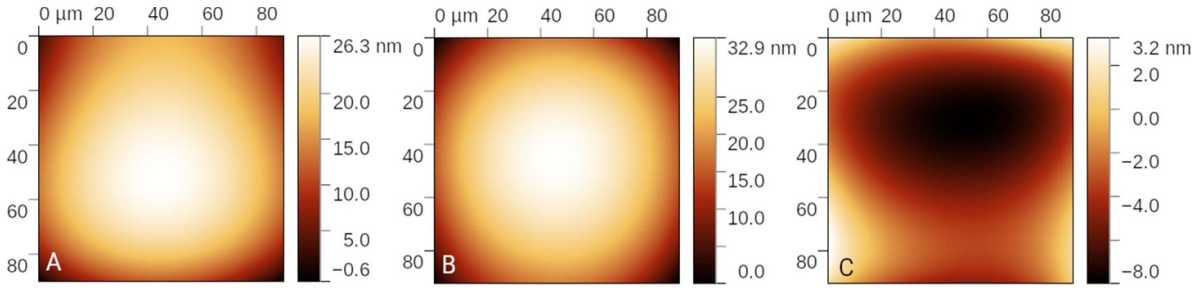

Figure 6. Commercial SPM scanner background determined from stitching (A), background determined from a series of measurements of a flat surface (B) and their difference (C).

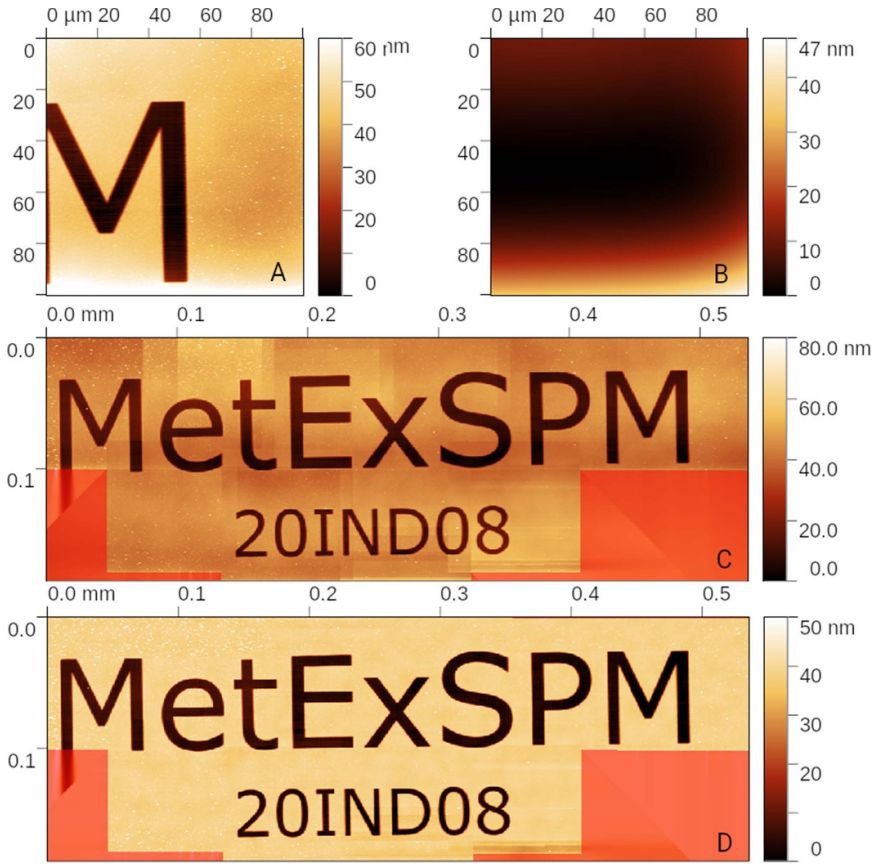

Figure 7. Stitching result from a commercial SPM with added interferometers: (A) sample image, (B) estimated polynomial background, (C) stitched result using polynomial background and (D) stitched result using flatten base algorithm. Red mask shows areas that were not measured.

As the absolute positions of the images in the set are determined by the interferometers, the lateral stitching results can be compared with the interferometer positions. This can be used to estimate a residual error in the microscope calibration. The dependence of the average lateral stitching shifts estimated for different additional calibration factors is shown in figure 8. While the accuracy of the estimated calibration factors in this particular data set, with a small number of stitched frames and quite flat topography, cannot be a substitute for a proper microscope calibration, the method can be used to transfer the traceability to the microscope scanner motion, albeit with uncertainty.

4.4. Metrological HS-AFM system

To show the methods' performance on a metrological high-speed SPM, two datasets were used that were obtained using the NPL HS-AFM showing topography of a numbered grating and a flatness standard. Examples of high-speed frames on both samples are shown in figure 9.

As the instrument uses interferometers to read the lateral positions of all the data points (combined positions of the coarse and fine stages), data from individual images should be ideally treated as a *XYZ* data set and simply merged together. However, as both the coarse positioning and high-speed stages

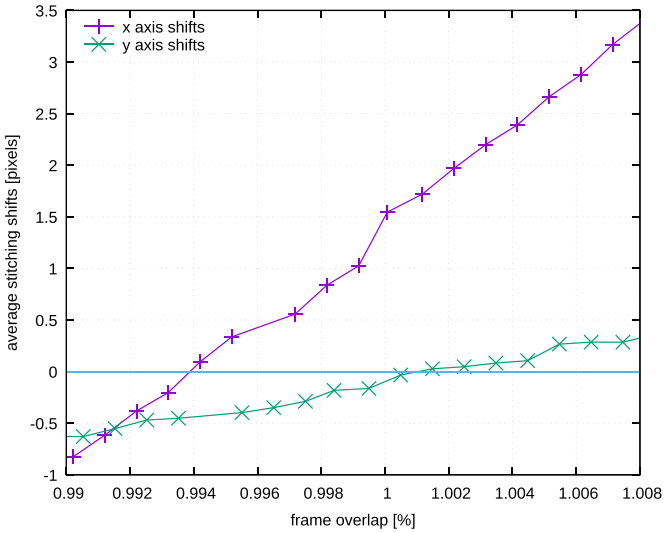

Figure 8. Microscope residual calibration error estimation via stitching. Intersection with zero line provides the optimal calibration factors.

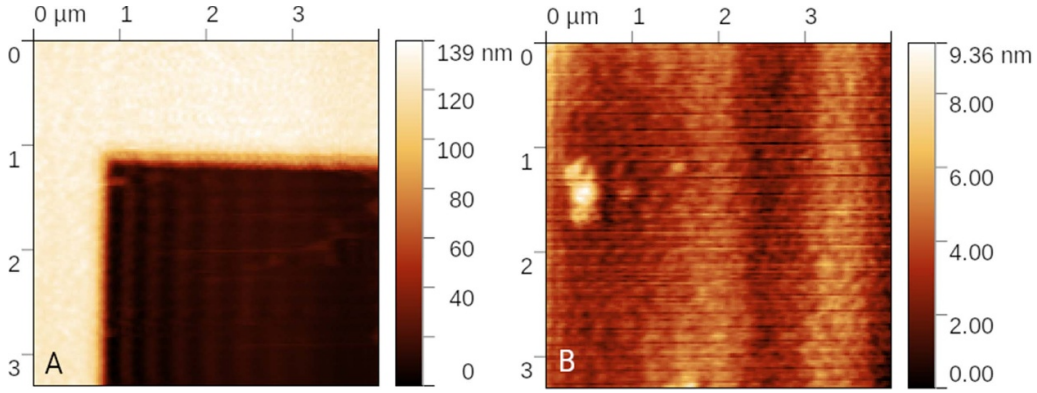

Figure 9. Individual frames from the numbered grating and the flatness standard measured by the NPL high-speed metrological AFM.

feature some unwanted z axis motion that is not currently measured, stitching in the z-axis is still required.

This was used as an opportunity to stitch a large dataset with relatively high levels of imperfections coming from high-speed scanning. Therefore, the individual frames were rasterised back to the regular grid, creating an image stack, using the centre positions as a guide for stitching using the same stitching methodology as for the data from the other microscopes.

The stitching process and stitching results for the numbered grating are illustrated in figure 10. When the nominal frame-to-frame lateral offset was 3 µm while the frame size was 4 × 3.4 µm, It can be seen that even with relatively small overlaps in the y axis, the stitching process works well.

The polynomial scanner background can also be estimated; however, as it can be seen from figure 9, backgrounds in high-speed images can be quite complex, containing also a non-negligible amount of vibrations coming from the scanner or cantilever, seen as vertical stripes, so a polynomial background contains both part of the mechanical vibration effects and the real scanner non-flatness.

A more detailed measurement is shown in figure 11, where just part of the grating was measured with higher overlaps (frame to frame lateral offset of 1 µm).

To investigate the performance of the scanner background subtraction methods further, a flatness standard measurement was used, shown in figure 12, together with the effects of different methods for background subtraction. It can be seen that polynomial background subtraction leads only to partial correction of the imperfections coming from the scanner. Using a mean frame as a background led to very similar results. The reason for this is that the background changed slightly during the scan. There is no single background image that could cover all these effects. This is why the average background (evaluated as a mean of all the images) does not help with stitching.

The best result was obtained when a flatten base algorithm was used for correction of all the individual frames. Even though it is still possible tosee some stitching residuals, the

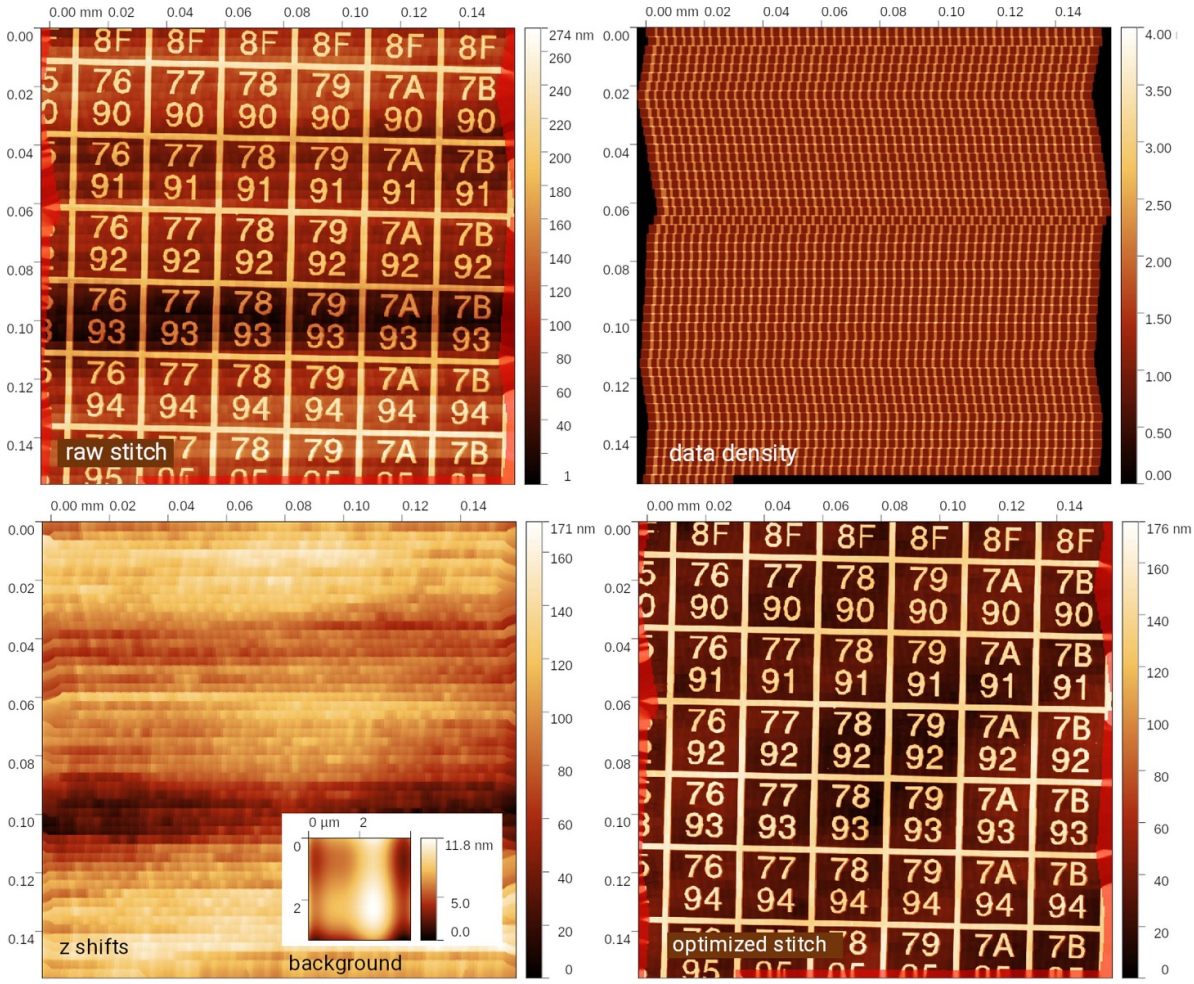

Figure 10. NPL numbered grating: raw stitch without polynomial background removal, data density, estimated z shifts and polynomial background (see inset) and stitching result.

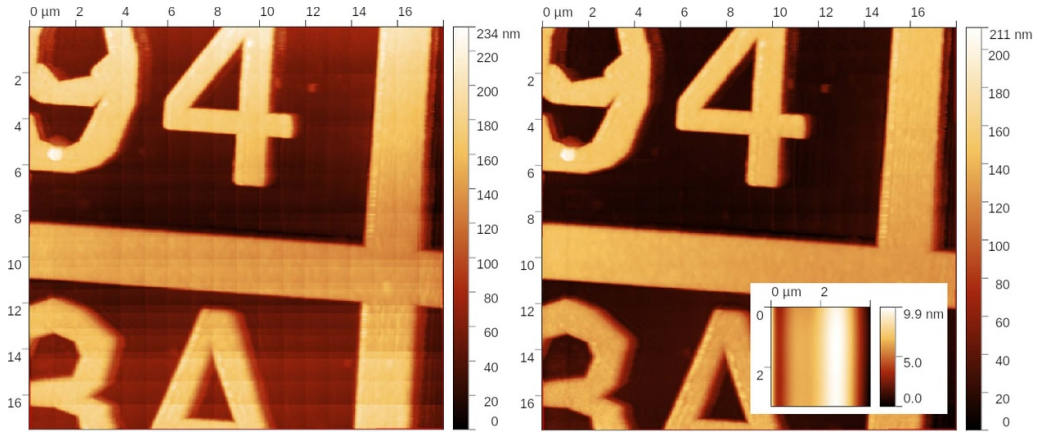

Figure 11. NPL numbered grating detail: raw stitch (left), polynomial background based stitch (right) and the detected polynomial background (inset).

resulting surface roughness in areas not containing visible dust particles is only 0.32 nm. However, flatten base is still a polynomial background subtraction method, it is just a bit 'smarter' with respect to specific features on the surface. Any polynomial background subtraction removes (or substantially suppresses) the long-wavelength components, regardless of whether they originate from scanner imperfections, sample form, or large scale roughness (waviness). They are all described by the same low-degree polynomials and, in general, impossible to separate.

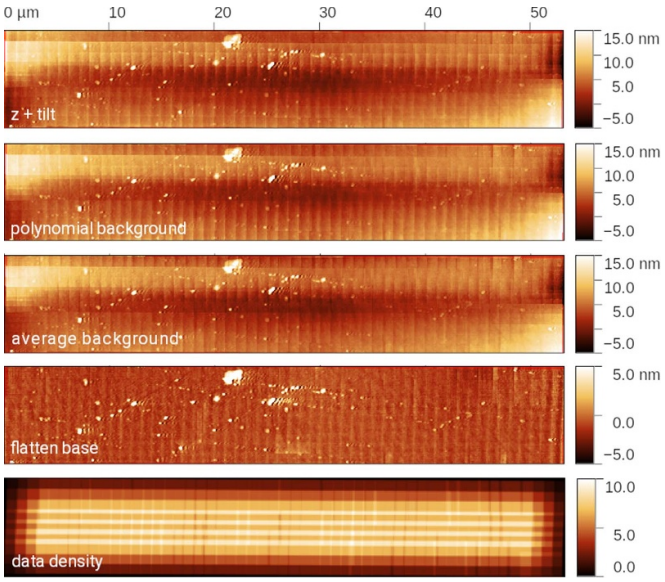

Figure 12. NPL flatness sample result for different background subtraction methods.

5. Conclusions

As with other types of microscopy, image stitching is an alternative to large area scanning for scanning probe microscopes. Using stitched images, an extremely large surface area can be imaged even with a commercial SPM that has a limited scan area. Factors affecting the limit of image size include performance of the larger mechanical loops, motion stage ranges and data storage capacity. The work in this paper has shown that:

(i) When data are stitched together, additional information can be extracted, e.g. related to the image scale and coarse sample positioning sensors' accuracy.
(ii) The ability to use stitching methods and their effect on the final accuracy of measurement is, not surprisingly, affected by the quality of the input data. The most critical problem is thermal and mechanical drift in the z axis during individual frame's acquisition and its evolution in time, which directly translates to the accuracy of stitched data in z.
(iii) When evaluating scanner background, other typical error sources, such as jumps in the z direction or line mismatch, should be minimised, as their correction can affect the estimated scanner background. Even if these effects were partly observed, stitching can provide results with errors in the single nanometre range.
(iv) Local data correction methods, like background flattening techniques, could also be successfully used if the user does not want to measure the scanner background during the stitching process. This, however, means that the result will have a flat background regardless of the real shape of the sample, which is acceptable if we want to evaluate local roughness or lateral dimensional quantities, but unsuitable if we focus on sample form or waviness. As such, it must be used with care and the user made aware of the caveats and limitations associated with its use.
(v) In the lateral direction, the lack of features for cross-correlation and image overlaps that are too small are the most significant sources of error. Use of interferometric sensors for the readout of coarse lateral positions in a coarse-fine stage system adds the possibility of creating a traceability link between positioning stages in the system, which in principle can be simpler than when calibration samples are used; however, care must be taken to consider the effects of interferometer non-linearity and the geometric configuration.
(vi) The large impact of z drift on the stitched data highlights the benefits of using high-speed SPM systems where individual frame measurements are performed fast enough to be almost drift-free. Even if the use of high-speed scanners creates additional challenges in minimising the mechanical vibrations, some part of these errors can be removed using a higher order polynomial background during stitching.

In summary, although stitching performance cannot beat that of fully metrological long-range systems, it has many benefits, offering a cost effective fast alternative that supports many applications of large area SPM imaging.

Data availability statement

The data that support the findings of this study are openly available at the following URL/DOI: https://doi.org/10.5281/zenodo.10728573.

Acknowledgments

The work was supported by the 20IND08 MetExSPM project that has received funding from the EMPIR programme co-financed by the Participating States and from the European Union's Horizon 2020 research and innovation programme. This work was additionally partly funded by the UK Government's Department for Science, Innovation & Technology through the UK's National Measurement System programmes. The authors would like to thank PTB for manufacturing and providing the MetExSPM sample.

Disclaimer

The naming of any manufacturer or supplier by the authors in this paper shall not be taken to be either the authors's endorsement of specific samples of products of the said manufacturer, nor recommendation of the said supplier. Furthermore, the authors cannot be held responsible for the use of, or inability to use, any products mentioned herein.

ORCID iDs

Petr Klapetek https://orcid.org/0000-0001-5241-9178
David Nečas https://orcid.org/0000-0001-7731-8453
Edward Heaps https://orcid.org/0000-0002-1794-1603
Bruno Sauvet https://orcid.org/0000-0002-0997-4579
Miroslav Valtr https://orcid.org/0000-0002-7628-9184
Virpi Korpelainen https://orcid.org/0000-0001-9123-8521
Andrew Yacoot https://orcid.org/0000-0001-6740-821X

References

[1] Strategy 2018-2028 consultative committee for length (CCL) 2018 (available at: www.bipm.org/documents/20126/2070984/CCL+Strategy.pdf/0f4af537-1729-b44a-e39e-f0023e439435)
[2] Dai G, Degenhardt J, Hu X, Wolff H, Tutsch R and Manske E 2023 A feasibility study towards traceable calibration of size and form of microspheres by stitching AFM images using ICP point-to-plane algorithm *Meas. Sci. Technol.* **34** 055009
[3] Manske E, Hausotte T, Mastylo R, Machleidt T, Franke K-H and Jäger G 2007 New applications of the nanopositioning and nanomeasuring machine by using advanced tactile and non-tactile probes *Meas. Sci. Technol.* **18** 520
[4] Werner C, Rosielle P C J N and Steinbuch M 2010 Design of a long stroke translation stage for AFM *Int. J. Mach. Tools Manuf.* **50** 183–90
[5] Eves B J 2009 Design of a large measurement-volume metrological atomic force microscope (AFM) *Meas. Sci. Technol.* **20** 084003
[6] Dai G, Wolff H, Pohlenz F and Danzebrink H U 2009 A metrological large range atomic force microscope with improved performance *Rev. Sci. Instrum.* **80** 043702
[7] Ortlepp I *et al* 2022 Nanofabrication and -metrology by using the nanofabrication machine (NFM-100) *Proc. SPIE* **12054** 120540A
[8] Klapetek P, Valtr M, Picco L, Payton O D, Martinek J, Yacoot A and Miles M 2015 Large area high-speed metrology SPM system *Nanotechnology* **26** 065501
[9] Heaps E, Yacoot A, Dongmo H, Picco L, Payton O D, Russell-Pavier F and Klapetek P 2020 Bringing real-time traceability to high-speed atomic force microscopy *Meas. Sci. Technol.* **31** 074005
[10] Dai G, Koenders L, Fluegge J and Hemmleb M 2018 Fast and accurate: high-speed metrological large-range AFM for surface and nanometrology *Meas. Sci. Technol.* **29** 054012
[11] Ando T 2012 High-speed atomic force microscopy coming of age *Nanotechnology* **23** 062001
[12] Picco L M, Bozec L, Ulcinas A, Engledew D J, Antognozzi M, Horton M A and Miles M J 2007 Breaking the speed limit with atomic force microscopy *Nanotechnology* **18** 044030
[13] Fantner G E *et al* 2006 Components for high speed atomic force microscopy *Ultramicroscopy* **106** 881–7
[14] Humphris A D L, Miles M J and Hobbs J K 2005 A mechanical microscope: High-speed atomic force microscopy *Appl. Phys. Lett.* **86** 034106
[15] Chalfoun J, Majurski M, Blattner T, Bhadriraju K, Keyrouz W, Bajcsy P and Brady M 2017 MIST: accurate and scalable microscopy image stitching tool with stage modeling and error minimization *Sci. Rep.* **7** 4988
[16] Preibisch S, Saalfeld S and Tomancak P 2009 Globally optimal stitching of tiled 3D microscopic image acquisitions *Bioinformatics* **25** 1463–5
[17] Bria A and Iannello G 2012 TeraStitcher - a tool for fast automatic 3D-stitching of teravoxel-sized microscopy images *BMC Bioinform.* **13** 316
[18] Yu Y and Peng H 2011 Automated high speed stitching of large 3D microscopic images *IEEE Int. Symp. on Biomedical Imaging: From Nano to Macro* (*Chicago, IL, USA*) pp 238–41
[19] Edwards H, McGlothlin R and Elisa U 1998 Vertical metrology using scanning-probe microscopes: imaging distortions and measurement repeatability *J. Appl. Phys.* **83** 3952–71
[20] Breil R *et al* 2002 Intercomparison of scanning probe microscopes *Precis. Eng.* **26** 296–305
[21] Yacoot A, Klapetek P, Valtr M, Grolich P, Dongmo H, Mattia G and Bridges A 2019 Design and performance of a test rig for evaluation of nanopositioning stages *Meas. Sci. Technol.* **30** 035002
[22] Klapetek P, Picco L, Payton O, Yacoot A and Miles M 2013 Error mapping of high-speed AFM systems *Meas. Sci. Technol.* **24** 025006
[23] Payton O, Picco L, Miles M, Homer M E and Champneys A R 2012 Improving the signal-to-noise ratio of high-speed contact mode atomic force microscopy *Rev. Sci. Instrum.* **83** 083710
[24] Yacoot A and Downs M J 2000 The use of x-ray interferometry to investigate the linearity of the NPL Differential Plane Mirror Optical Interferometer *Meas. Sci. Technol.* **11** 1126
[25] Valtr M, Klapetek P, Martinek J, Novotný O, Jelínek Z, Hortvík V and Nečas D 2023 Scanning Probe Microscopy controller with advanced sampling support *HardwareX* **15** e00451
[26] Nečas D and Klapetek P 2012 Gwyddion: an open-source software for SPM data analysis *Cent. Eur. J. Phys.* **10** 181–8
[27] Klapetek P, Yacoot A, Grolich P, Valtr M and Nečas D 2016 Gwyscan: a library to support non-equidistant scanning probe microscope measurements *Meas. Sci. Technol.* **28** 034015
[28] Klapetek P 2018 *Quantitative Data Processing in Scanning Probe Microscopy* 2nd edn (Elsevier) (https://doi.org/10.1016/C2011-0-09615-15-1)
[29] Nečas D and Klapetek P 2021 Synthetic data in quantitative scanning probe microscopy *Nanomaterials* **11** 1746